Journal of Power Sources 256 (2014) 369–382

Contents lists available at ScienceDirect

Journal of Power Sources

journal homepage: www.elsevier.com/locate/jpowsour

A generalized multi-dimensional mathematical model for charging and discharging processes in a supercapacitor

S. Allu [a,*], B. Velamur Asokan [b], W.A. Shelton [c,d], B. Philip [a], S. Pannala [a,*]

[a] Oak Ridge National Laboratory, Computer Science and Mathematics Division, 1 Bethel Valley Road, Oak Ridge, TN 37831, USA
[b] Exxonmobil Upstream Research Company, Houston, TX 77098, USA
[c] Cain Department of Chemical Engineering, Louisiana State University, Baton Rouge, LA 70803, USA
[d] Center for Computation and Technology, Louisiana State University, Baton Rouge, LA 70803, USA

HIGHLIGHTS

- Generalized 3D computational model of an electric double layer supercapacitor.
- 3D microstructural aspects do not have a significant impact on the performance.
- Specific capacitance, ionic conductivity, and tortuosity are critical.
- State-of-the-art numerical methods provide accurate and robust solutions.

ARTICLE INFO

Article history:
Received 18 November 2013
Received in revised form
11 January 2014
Accepted 13 January 2014
Available online 23 January 2014

Keywords:
Supercapacitors
Computer modeling
Electrochemical modeling
Multidimensional simulations
Energy storage

ABSTRACT

A generalized three dimensional computational model based on unified formulation of electrode–electrolyte system of an electric double layer supercapacitor has been developed. This model accounts for charge transport across the electrode-electrolyte system. It is based on volume averaging, a widely used technique in multiphase flow modeling ([1,2]) and is analogous to porous media theory employed for electrochemical systems [3–5]. A single-domain approach is considered in the formulation where there is no need to model the interfacial boundary conditions explicitly as done in prior literature ([6]). Spatio-temporal variations, anisotropic physical properties, and upscaled parameters from lower length-scale simulations and experiments can be easily introduced in the formulation. Model complexities like irregular geometric configuration, porous electrodes, charge transport and related performance characteristics of the supercapacitor can be effectively captured in higher dimensions. This generalized model also provides insight into the applicability of 1D models ([6]) and where multidimensional effects need to be considered. A sensitivity analysis is presented to ascertain the dependence of the charge and discharge processes on key model parameters. Finally, application of the formulation to non-planar supercapacitors is presented.

© 2014 Elsevier B.V. All rights reserved.

1. Introduction

Ultracapacitors or supercapacitors are charge storage devices that operate on the principle of electrochemical double layer (ECDL) capacitance wherein, electrical energy can be stored and released by nanoscale charge separation at the interface between the electrode and the electrolyte. In paper [7] advances in electrode materials for the supercapacitor are summarized. There has been considerable activity in the recent years to exploit high surface area offered by Nanotubes [8–14] and more recently Graphene [15]. Most of the projected gains in energy densities (getting closer to that of current Li-ion batteries) are due to increase in capacitance through increase in surface area and exploiting the nano-pore and ion interactions. However, considerable development needs to be done at the system level to ascertain the true performance in a practical supercapacitor [16]. In this work, we developed a macroscopic model that can rapidly use the microscale properties to assess the overall performance of the supercapacitor device and possibly aid in transition of this rapid progress in supercapacitor electrode materials into high performance supercapacitors without lot of iterations at the device level where one needs to balance the cathode, anode, electrolyte, and current collectors to maximize energy and power density.

* Corresponding authors.
E-mail addresses: allus@ornl.gov (S. Allu), badri.velamur.asokan@exxonmobil.com (B. Velamur Asokan), shelton@lsu.edu (W.A. Shelton), philipb@ornl.gov (B. Philip), pannalas@ornl.gov, pannalas@gmail.com (S. Pannala).

0378-7753/$ – see front matter © 2014 Elsevier B.V. All rights reserved.
http://dx.doi.org/10.1016/j.jpowsour.2014.01.054

Advantages in using the nanoporous carbon materials with fine tuned pore sizes for the corresponding electrolytes is well established. Especially, the cathode and anode with different pore sizes that match the anion and cation sizes could lead to improved power delivery. Aspects such as high conductivity and surface area of these carbon material characteristics are studied for various engineered carbon material with tailored pore-size distribution for high capacitance [10,11,17].

The amount of energy stored in a supercapacitor is inversely proportional to the thickness of the double layer and directly proportional to the specific surface area of the electrodes. By using nanoporous electrodes, supercapacitors deliver a sufficiently high power density compared to conventional batteries and an extremely high energy density compared to conventional dielectric capacitors. However, the energy density of supercapacitor devices are an order of magnitude lower than current battery devices.

They are also amenable to a variety of applications ranging from energy-smoothing, regenerative braking to power-source in hybrid vehicles. Supercapacitors have the advantage of long operating life, a wide thermal operating range, low weight, low maintenance and near infinite cyclability (charge–discharge).

A Ragone plot (see Fig. 1) shows the power density vs. energy density for common energy storage/conversion devices.

Currently, ultracapacitors need coupling with batteries to supply energy for a prolonged time period [18]. One of the motivations for developing novel materials is to increase their energy density and better simulation models can accelerate the adoption of the most promising materials from a full system perspective. In addition, several new designs at the system level can be explored to maximize the energy density while retaining very high power density and life. This requires a careful understanding of the physics at the nanoscale as well as the device scale. While there is a significant increase in research at the nanoscale [11,12,19,20], there is much work to be done at the device scale. Even recent publications e.g. Ref. [6] still consider the electrode properties to be isotropic and the simulations are done in one-dimension. With the advent of new graphene based electrode materials that are utilized for the ultracapacitor [21], due to its high surface area such as 2630 $m^2 g^{-1}$ [22], the accuracy of these assumptions with reference to truly nanostructured materials like chemically modified graphene and carbon nanotube solids have not been addressed. Also, most of these models assume the capacitance in the electrode pores (due to ECDL) can be modeled using parallel-plate assumption. It has been shown recently that capacitance exhibits a strong dependence with pore size and curvature [11,20]. Lanzi and Landou [23] show macroporous structure is important in determining the ohmic and mass-transfer resistance whereas in micropores these effects are negligible because transport is too localized. They also find that distribution in pore volume between macropores and micropores can have a major effect on porous electrode performance. Increase in porous material surface area for different activated carbon material and its influence to the capacitor performance i.e., specific capacitance, one of the important characteristics of the carbon electrode material, has been established [24,25].

In this paper, we test the validity of the first assumption, namely, the effect of anisotropy in electrode properties on the capacitance, charge and discharge characteristic of a ultracapacitor.

For our model, we consider an ultracapacitor unit-cell as shown in Fig. 2 comprising of two nanoporous electrodes isolated from electrical contact through a porous separator. The pores are filled with an electrolyte that allows ionic current to flow through the electrodes while preventing self-discharge. Current collectors typically made of metal foils drain the electrical current from each electrode. In a full-scale system, multitude of these unit-cells are used. For our modeling purpose, it is sufficient to characterize one of these unit-cells.

A historical perspective on modeling electrode-electrolyte interface as circuit has been presented by Geddes [26]. The macroscopic models are primarily based on electrical circuit models or simple 1D/pseudo-2D models [27,28]. V. Srinivasan and J. W. Weidner [29] developed analytical models for the capacitors under constant current while neglecting the electrode kinetics. Pillay and Newman [30] have studied the influence of side reactions using Tafel kinetics on performance of EDCL. A mathematical model is proposed by Ong and Newman [31] for double layer capacitor and the predictions show slower charge build-up due to double layer

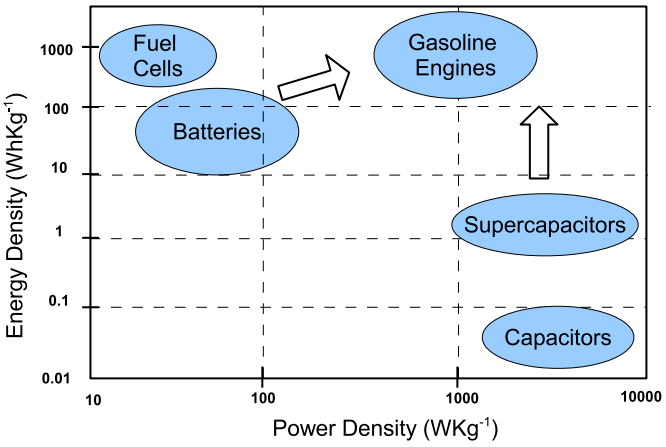

Fig. 1. A Ragone chart showing the power vs. energy densities for a number of energy storage devices and compares that to a gasoline engine. It can be noticed that ultracapacitors have almost 1000 times the energy density of dielectric capacitors and around 10 times the power density of conventional batteries. Units in this figure have been modified to be consistent with the journal requirement.

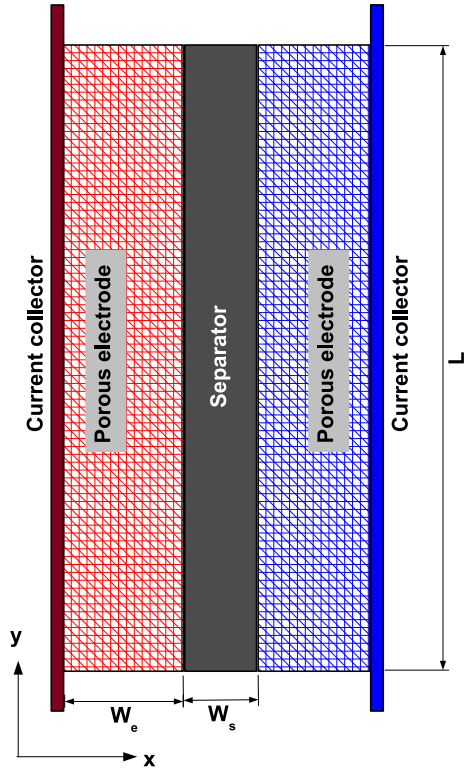

Fig. 2. Schematic of an electrochemical double-layer supercapacitor. The electrodes are typically made of a nanoporous material. The porous separator and the electrode pores are saturated with the electrolyte.

capacitance during galvanostatic charge. Also their analysis indicated no difference to the chemical kinetics model on the potential profiles. A new RC circuit model was proposed by Dunn and Newman [32] for the double-layer capacitors and maximum theoretical specific energy over a range of discharge times for constant-current and constant-power discharges were predicted by optimizing the electrode thickness, electrode porosity, and final voltage. Further modeling was done by Verbrugge and Liu [6] to include the microstructure and pore size distribution in calculating the effective properties of the porous electrodes.

The modeling technique adopted in these works allows for splitting the operator in each domain. Then solution to these individual operators are obtained by solving them in segregated fashion. Though solutions are obtained quickly, these segregated solution techniques give rise to numerical instabilities and convergence issues. The main problem might be the fact that the strongly elliptic equations have been solved as parabolic/hyperbolic equations by segmenting the domain and specifying hand-shake boundaries at the interfaces. This leads to ill-posed numerical scheme where iterative techniques may not converge and solutions are not assured in all possible problem setups.

These models are limited in their ability to capture spatial variations in permeability or conductivity or able to handle multidimensional structure of the electrode material. Any variations in the porosity of the solid material or anisotropy of the physical properties are not accounted. All previous models have assumed a single value of electrode porosity and have not considered the effect of varying pore structure, electrode composition on electrochemical capacitor performance [33]. Also, the temporal changes of the transport properties are neglected in the simulations.

1.1. Scope of present work

In this paper we propose a unified multi-dimensional formulation across the electrode-electrolyte-electrode system using a volume averaging approach typical of multiphase flow formulation ([1,2]) and is similar to the porous media theory often used for modeling batteries [3–5]. Following are some of its advantages over the 1D models:

- General multi-dimensional formulation allowing for realistic 2D and 3D effects
- Anisotropic electric and heat conductance, capacitance, chemistry etc. can be specified as a function of space and time
- This formulation is also suitable for any upscaling from lower length- and time-scale methods as the properties can be determined locally (at the discretization level)
- Because of the single-domain approach, complex geometries are naturally incorporated. The same formulation applies to 1D, 2D and 3D geometries irrespective of the complexities associated with dimensionality as well as with electrode/electrolyte spatial arrangements
- Unlike previously used methods for supercapacitors based on a segregated formulation with intermediate boundaries, by having a unified, single-domain approach, stability and convergence of the numerical algorithm is fundamentally guaranteed
- Implicit coupled solutions can be obtained with improved numerical efficiency and can be scaled to run of massively parallel computers as needed

We first validate this unified approach by comparing with experiments reported in the literature to verify the accuracy and efficiency of the method. Furthermore, we have tested some of the assumptions made currently in terms of isotropy, homogeneity etc., to understand the sensitivity to the overall performance of the supercapacitor but also to the internal fields such as local potential and current within the cell. We also applied this method to a 2D supercapacitor configuration to study the effects of non-planar arrangements.

To arrive at the governing equations at the device scale, we use the volume averaging approach wherein, the electrode/separator and the electrolyte are considered as inter-penetrating continua. Individual conservation equations for each phase are averaged over a volume element that is larger than the pore scale and smaller than the device scale (here, the electrode thickness). Clearly, this requires that the microscopic features of the electrode be more or less uniform and at a length scale much smaller than the rest of the domain. This requirement can be violated for truly nanostructured materials e.g., in CNT solids, the pores can extend right through the electrode. Thus averaging along the thickness of the electrode is not valid. This is an extreme case and we shall assume that the effect of nanoscale structures can be captured by considering anisotropy in the electrode material properties.

We also assume the dilute-solution theory for the liquid phase in the pores of the electrode. This assumption is validated since the salt concentration in the electrolyte is small enough ($<$1 M) and that the electrolyte conductivity is a linear function of the salt concentration in that regime [6]. Furthermore, little information is available on the concentration dependence of the physical and chemical parameters of the system. As more information about the parameters is available for e.g., through ab-initio simulations, this assumption has to be revisited.

This paper is structured as follows: In the next section, a mathematical model for the ECDL is provided with a brief discussion on its validity. Following this, the analysis for the case of a uniform property, isotropic, binary electrolyte is provided. Results are compared with literature. We then, consider the case of anisotropy and spatial variability in the matrix properties (which also effects liquid phase properties through porosity variations). Finally, we present results from a 2D supercapacitor configuration followed by conclusions.

2. Mathematical model

To derive the volume-averaged mathematical model, we start with the conservation of charge for a infinitesimal volume element inside the supercapacitor:

$$\frac{\partial}{\partial t} q + \nabla \cdot J = 0 \tag{1}$$

where, q is the charge contained in the volume element and J is the current density that acts as a flux term on the boundaries of the volume element. By Nernst–Planck relation, for a given electrolyte, there are three possible modes that can affect the current density: a) voltage gradients, b) concentration of different species, and c) external velocities (for species convection). In this paper, for simplicity, we only consider supercapacitors with no chemical reactions or external forcing terms and the framework can be easily extendable to include chemical reactions and external forcing. Therefore, the current density can be modeled according to Ohm's law. Before we can derive the supercapacitor model, we need a few preliminaries:

Volume fraction: The volume fraction of a component is calculated as

$$\epsilon_k = \frac{\mathrm{d}V_k}{\mathrm{d}V} \tag{2}$$

where, $\mathrm{d}V$ is the volume of the infinitesimal volume element and $\mathrm{d}V_k$ is the volume occupied by the k-th phase/species in that

element. Let us now consider the volume average of the charge conservation equation Eq. (1)

$$\frac{\partial}{\partial t}\langle q\rangle + \langle \nabla\cdot J\rangle = 0,$$
$$\text{where averaging operator} \langle g\rangle = \int_{dV} g d\Omega \tag{3}$$

In the L.H.S, it is tacitly assumed that the volume element does not vary with time, i.e., there is no dilatation. Let us now consider physical models for the various terms in the above equation.

Model for q: In a supercapacitor, the capacitance arises from charge separation across the double layer that occurs at the interface of the electrode and electrolyte. Let the local capacitance in the volume element be C and the local voltage across the double layer be $\tilde{V}$. In this volume averaged approach, we are capturing the effect of the double layer while explicitly not resolving the interface between the electrode and electrolyte. We have local charge density as $q = C\tilde{V}$. On taking the volume average, we get $\langle q\rangle = \langle C\rangle\langle\tilde{V}\rangle + \langle C'\tilde{V}'\rangle$. Where, C' and $\tilde{V}'$ are the fluctuations in the local capacitance and voltage due to spatial variations of the electrode microstructure and properties below the resolution of the volume element. Currently, only the averaged capacitance of a supercapacitor is measured and these spatial variations are not available. One could perform simulations analogous to DNS (Direct Numerical Simulations) for batteries [34], where the supercapacitor morphology along with the double layer can be explicitly resolved to provide these closures. For now, we assume that $C' = 0$ and this additional term can be included once we have more data. This yields:

$$\langle q\rangle = C\tilde{V}, \quad \text{where} \quad C = \langle C\rangle, \tilde{V} = \left\langle \tilde{V}\right\rangle \tag{4}$$

Model for J: The Ohm's law for a given component (electrode or electrolyte) can be written to be of the following form

$$J_\alpha = -k_\alpha \nabla V_\alpha \tag{5}$$

where, J_α is the current density, V_α is the local potential, and k_α is electrical conductivity within the material component α. By volume averaging the above equation and utilizing the definition of volume fraction, we get:

$$\langle J\rangle = -(k_\alpha\epsilon_\alpha)\nabla V_\alpha + \langle k'\nabla V'_\alpha\rangle \tag{6}$$

where the fluctuation term again represents the unresolved fluctuations due to the variations in microstructure and properties below the volume element that we do not explicitly model. Though this term could be of considerable importance to understand local variations, due to lack of knowledge about the microstructure of the electrodes or how the properties vary at those scales, we neglect this term. Since, we are interested in the mean response of the supercapacitor at the coarse scales and the dominant (diffusion) operator is linear, this is not a bad assumption in terms of capturing overall response of the system. Here we wanted to have a general derivation so that we can include additional details when available and also provide a way to link to lower length-scale simulations or experiments that resolve the small scale variations.

This brings us to the model equation

$$C\frac{\partial}{\partial t}\tilde{V} = \nabla\cdot((k_\alpha\epsilon_\alpha)\nabla V_\alpha) \tag{7}$$

The above equation is valid over each component and assumes C does not vary with time. If C varies with time, the above formulation will be slightly modified with C moving into the time derivative term. For a full-cell simulation, one needs to formulate in terms of the potential in the neutral phase of the electrolyte and electrode materials. We note that conservation of current is ensured i.e., $i_1 + i_2 = 0$ and no species gradient is assumed which is true for the region outside of electric double layer. These governing equations can be written as follows:

$$C\frac{\partial}{\partial t}(V_l - V_s) = \nabla\cdot(k_l\epsilon_l\nabla V_l) \tag{8}$$

$$C\frac{\partial}{\partial t}(V_s - V_l) = \nabla\cdot(k_s\epsilon_s\nabla V_s) \tag{9}$$

This set of equations model any change of potential in electrode phase and a corresponding automatic response of the potential in electrolyte phase to ensure charge neutrality. The multi-domain specific equations used in Ref. [6] reduce to this form and both formulations are consistent. The biggest advantage of the current formulation is that these set of equations are applicable over the entire supercapacitor and the local volume fraction and corresponding phasic properties ensures the consistency between these two different formulations. We can therefore only specify the boundary conditions at the current collectors and treat complex 2D and 3D configurations easily as we do not have to explicitly handle internal domain boundaries.

2.1. Numerical solution procedure

In this section we briefly describe the solution procedure employed in solving the system of Eqs. (8) and (9) for charge conservation in electrochemical double layer super-capacitor.

These equations are discretized in time using first-order BDF (backward differentiation formula) and in space using standard finite element method. For the discretization based on finite element formulation we begin with the system of equations,

$$\left.\begin{aligned} C\tfrac{\partial}{\partial t}(V_l - V_s) &= \nabla\cdot(k_l\epsilon_l\nabla V_l)\\ C\tfrac{\partial}{\partial t}(V_s - V_l) &= \nabla\cdot(k_s\epsilon_s\nabla V_s)\end{aligned}\right\} \quad \text{in} \quad \Omega_{xt} \tag{10}$$

with boundary conditions,

for galvanostatic charge:

$$\begin{aligned}\sigma_s\epsilon_s\tfrac{\partial V_s}{\partial n} &= -i_0 \quad \text{on} \quad \Gamma_1\\ \sigma_s\epsilon_s\tfrac{\partial V_s}{\partial n} &= i_0 \quad \text{on} \quad \Gamma_2\end{aligned} \tag{11}$$

for potentiostatic discharge:

$$\begin{aligned}V_s &= -V_0/2 \quad \text{on} \quad \Gamma_1\\ V_s &= V_0/2 \quad \text{on} \quad \Gamma_2\end{aligned} \tag{12}$$

where $\Gamma_1\overline{\cup}\Gamma_2 = \Gamma = d\Omega$ and $\Gamma_1\cap\Gamma_2 = \varnothing$

We construct an integral form based on Galerkin Method with weak form by transferring one order of differentiation from $V = \{V_l, V_s\}$ to test function w,

$$\begin{aligned}\int_\Omega\left(C\frac{\partial(V_l - V_s)}{\partial t}\right)w d\Omega + \int_\Omega (k_l\epsilon_l\nabla V_l\nabla w)d\Omega &= wk_l\epsilon_l\cdot\nabla V_l\big|_\Gamma\\ \int_\Omega\left(C\frac{\partial(V_s - V_l)}{\partial t}\right)w d\Omega + \int_\Omega (k_s\epsilon_s\nabla V_s\nabla w)d\Omega &= wk_s\epsilon_s\cdot\nabla V_s\big|_\Gamma\end{aligned} \tag{13}$$

This constitutes the weak form in Ω_x. Let $\overline{\Omega}_x = \cup_e\overline{\Omega}_x^e$ be the discretization of $\overline{\Omega}_x$ in which $\overline{\Omega}_x^e$ is an element e. Now consider the element approximation for $\{V\}$ such that

$$V_h^e(x,t) = \sum_i^N N_i(x) V_i^e(t) = [N(x)]V^e(t) \tag{14}$$

Using this Eq. (14) we can write

$$\begin{aligned} \frac{\partial V_h^e}{\partial x} &= \sum_{i=1}^{n} \frac{\partial N_i(x)}{\partial x} V^e(t) = \frac{\partial [N]}{\partial x} V^e \\ \frac{\partial V_h^e}{\partial t} &= \sum_{i=1}^{n} N_i(x) \frac{\partial V_i^e(t)}{\partial t} = [N]\dot{V}^e \end{aligned} \tag{15}$$

Substituting these relations into Eq. (13) we get,

$$\begin{aligned} &\int_{\Omega_x^e} CN_j[N]\left(\dot{V}_l^e - \dot{V}_s^e\right) d\Omega_x + \int_{\Omega_x^e} k_l \epsilon_l \frac{\partial N_j}{\partial x}\left(\frac{\partial N}{\partial x} V_1^e\right) d\Omega_x \\ &= N_j(x_{e+1}) k_l \epsilon_l \nabla V_l\Big|_{x_{e+1}} - N_j(x_e) k_l \epsilon_l \nabla V_l\Big|_{x_e} \end{aligned} \tag{16}$$

$$\begin{aligned} &\int_{\Omega_x^e} CN_j[N]\left(\dot{V}_s^e - \dot{V}_l^e\right) d\Omega_x + \int_{\Omega_x^e} k_s \epsilon_s \frac{\partial N_j}{\partial x}\left(\frac{\partial N}{\partial x} V_2^e\right) d\Omega_x \\ &= N_j(x_{e+1}) k_s \epsilon_s \nabla V_s\Big|_{x_{e+1}} - N_j(x_e) k_s \epsilon_s \nabla V_s\Big|_{x_e} \end{aligned} \tag{17}$$

This can be written as,

$$C\left[I^k\right][M^e]\left\{\dot{V}^e\right\} + [D^e]\{V^e\} = \{P^e\} \tag{18}$$

where I^k is the block matrix for each component $\{V_l^e, V_s^e\}$ given by,

$$= \begin{bmatrix} 1 & -1 \\ -1 & 1 \end{bmatrix} \tag{19}$$

and

$$\begin{aligned} m_{ij}^e &= \int_{\Omega^e} N_i N_j d\Omega = \int_{-1}^{1} N_i N_j J d\xi \\ d_{ij}^e &= \int_{\Omega^e} \frac{\partial N_i}{\partial x}\frac{\partial N_j}{\partial x} d\Omega = \int_{-1}^{1} \frac{1}{J}\frac{\partial N_i}{\partial xi}\frac{\partial N_j}{\partial xi} d\xi \end{aligned}$$

For discretization in time, we use standard first order BDF scheme on $\{\dot{V}^e\}$ which results into following algebraic system,

$$\left\{C\frac{[M]}{\Delta t} + [D]\right\}\{V^e\}_{n+1} = \frac{[M]}{\Delta t}\{V^e\}_n + \{P\} \tag{20}$$

The strongly coupled formulation is implemented within Advanced Multi-Physics (AMP) software framework [35]. We use the standard interface to the Trilinos direct sparse linear solver [36] through AMP to solve the coupled algebraic system (20) for $\{V^e\} = \{V_l^e, V_s^e\}$.

3. Results

In this section, we use a commercial pseudocapacitor (see Table 1 for baseline properties) as a demonstration vehicle to present a number of studies that employ the formulation detailed above and highlight the flexibility and applicability of the proposed model. First, we validate the charging and discharging profiles by comparing to the experimental results. We will also present the grid refinement and convergence studies to demonstrate the accuracy of the solutions. Subsequent to these studies we will present a set of parametric studies to show the sensitivity of the results to different properties, anisotropy of both physical and geometric properties, and effects of non-planar architectures.

The simulations are all carried out with a current of 100 A for a variety of charging and discharging voltages. The numerical studies are divided into following sections.

Table 1
Properties and parameters for the simulations.

Parameter	Value	Units
Electrode width, W_e	50	μm
Separator width, W_s	25	μm
Electrode height, L	25	μm
Specific capacitance, aC	86	F m^{-3}
Void volume fraction in electrodes, ϵ_s	0.67	
Void volume fraction in separator, ϵ_l	0.6	
Electrolyte conductivity, κ	0.067	S m^{-1}
Solid phase conductivity, σ	52.1	S m^{-1}
Tortuosity for liquid phase in carbon electrode, τ_s	2.3	
Tortuosity for liquid phase in separator, τ_l	1.29	

3.1. Experimental validation

For model validation, we use the data from the 3500 F SAFT America supercapacitor (Maximum voltage 2.8 V) that was extensively studied earlier by Verbrugge and Liu [6]. This single cell supercapacitor consists of two carbon electrodes and a separator preventing physical contact between them. The physical properties used for the simulation are mostly derived from Ref. [6] and can be found in Table 2.

3.1.1. Comparison against the results from Verbrugge and Liu [6]

In Fig. 3, we compare the simulated supercapacitor voltage against the experimental results published in Ref. [6] for constant current charging from 1.6 V to 2.2 V. For the first 18 s of the simulation during this charge phase, the cell voltage increased from 1.6 V to 2.2 V. The charging time corresponding to the threshold voltage of 2.2 V matches very well. At this point, the boundary conditions are switched to constant voltage discharge at 1.4 V. In Fig. 4, we see a comparison of the current from the simulations to that of the experiment. The rapid initial rapid discharge followed by slow discharge asymptotically approaching zero current are accurately captured by the simulations and are in very good agreement with the experiments. This analysis gives us confidence that the current formulation captures the macroscopic response of the supercapacitor very well and we can use this model to further understand the sensitivities to grid refinement, model parameters, etc.

Table 2
Boundary conditions.

Left current collector ($x = 0$)	Right current collector ($x = L$)
Galvanostatic charging	
$\delta V_l/\delta x = 0$	$\delta V_l/\delta x = 0$
$V_s = 0$	$\delta V_s/\delta x = i_0/(\sigma\epsilon)$
Potentiostatic discharging	
$\delta V_l/\delta x = 0$	$\delta V_l/\delta x = 0$
$V_s = -V_{\text{discharge}}/2$	$V_s = V_{\text{discharge}}/2$

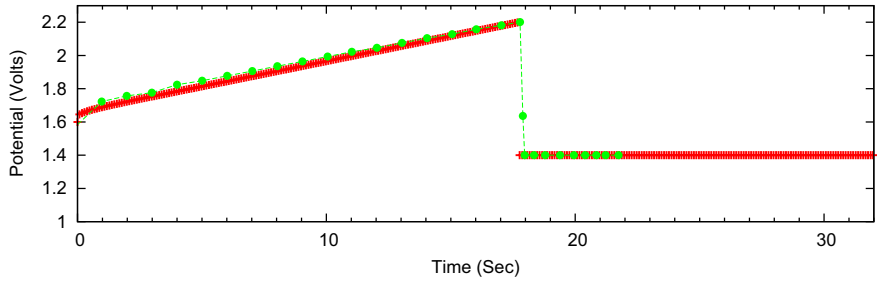

Fig. 3. Comparison of cell potential with the Verbrugge and Liu [6] results. The experiments are denoted by filled circles and simulations are + symbol.

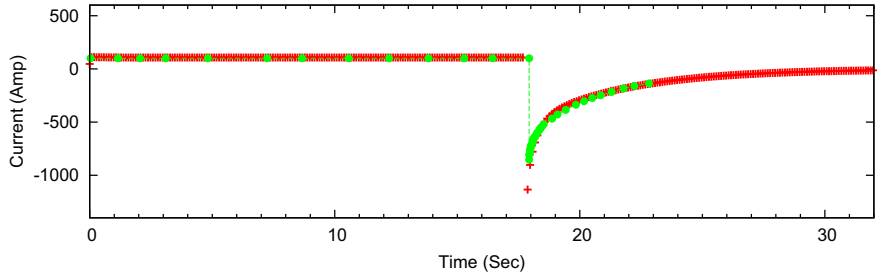

Fig. 4. Comparison of discharging current with the Verbrugge and Liu [6] results. The experiments are denoted by filled circles and simulations are + symbol.

3.1.2. Grid refinement and convergence

In Fig. 5, we show a mesh refinement study conducted to evaluate the convergence of the solution. For this study we have used three different meshes with 1200 and 2500 elements across the domain. The residual in the solution is of the $O(10^{-8})$ during the entire transient analysis. This shows that we have obtained grid independent solutions and any further refinements would not change the solution significantly.

The supercapacitor problem we are modeling is essential 1D and we are modeling it as a 2D system with few elements in the transverse direction. For generality one could also model it as a 3D system. In Fig. 6, we compare the cell potential and current density between 3D and 2D domains. As expected, the solutions are nearly identical as there are no gradients imposed in the third dimension. This verifies that the formulation for higher dimensions yields the same result as 2D and 1D if the inherent problem is of a lower dimension. This verification test ensures that both the formulation and the implementation are consistent to the physical processes we are modeling in the device.

3.1.3. Spatial variation of the potential and current density

A series of charge and discharge conditions are imposed to evaluate the solution characteristics of the supercapacitor. Initially, a potentiostatic charge is imposed to maintain a cell potential of 1.6 V and to equilibrate any initial gradients in the cell. At this stage, a galvanostatic charge of 100 A i.e, current density 64.93 Am^{-2} is imposed for charging the cell. This charging is continued until the cell potential reaches 2.2 V. The cell potential (difference across the cell) varies in time from 1.6 to 2.2 V but there are internal voltage gradients due to finite transport coefficients. Fig. 7 shows these variations along the width of supercapacitor and small gradients in voltage are established – these gradients are very minimal compared to overall cell voltage. After the cell reaches 2.2 V, the cell is subjected to a potentiostatic discharge at 1.4 V. As can be seen in Fig. 8, the gradients of the potential within the cell can be quite severe because of high current discharge during the switch from galvanostatic charge to potentiostatic discharge. Usually gradients are detrimental in terms of life and efficiency (under utilizing electrodes and losses)

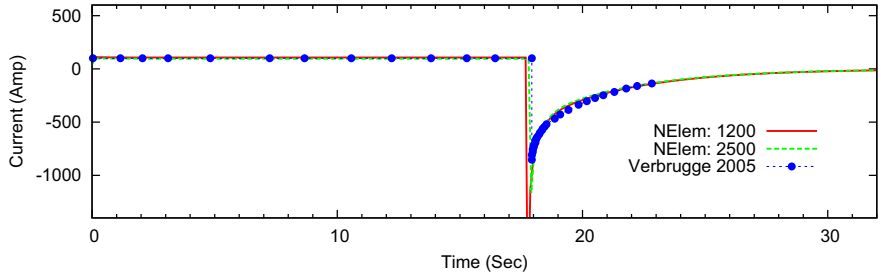

Fig. 5. Mesh convergence study.

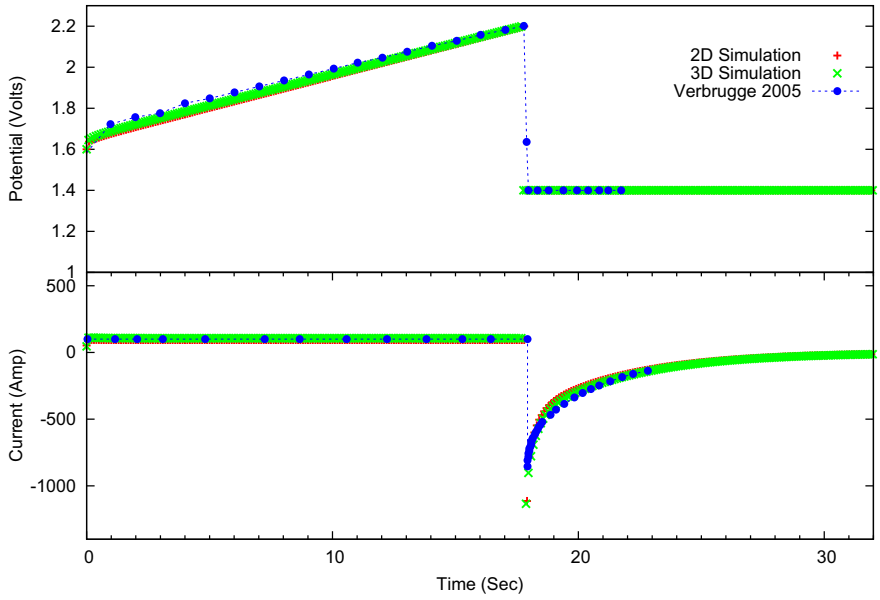

Fig. 6. Comparison of the charge/discharge profile from 3D to 2D domains.

and simulations such as these can identify operating conditions to minimize spatial gradients.

3.2. Sensitivity analysis to physical properties

In this section, we look at the sensitivity of the supercapacitor performance to variations in electronic conductivity in the electrode (σ), ionic conductivity in the electrolyte (κ), specific capacitance (aC), and Bruggeman's coefficient (tortuosity of the pore structure) as these are properties one can dial in using various advances in materials science. The purpose of such a parametric analysis is many folds: a) to understand what properties are to be measured accurately to get accurate simulation results, b) narrow down fundamental exploration to concentrate on variations that will have maximum impact on the overall system performance and c) to understand the relative interaction between the various competing properties. Below, we fix the void fraction in electrodes (ϵ_s), void fraction in separator (ϵ_l) corresponding to the base case we detailed before and vary one of the properties (σ, κ, or aC) relative to the base case. One could perform second order variations by changing two or more properties at the same time but we have not done that in this study.

Porous carbon with high surface area are prepared by various manufacturing processes [37,38]. The effective electronic conductivity of these materials hugely depends on the pore structure and compositions [39]. For the various configurations of

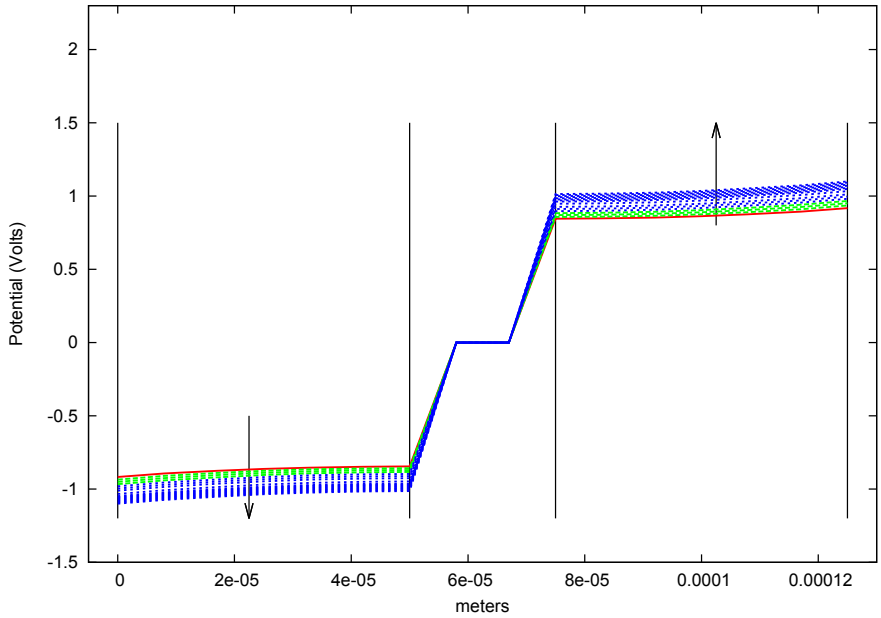

Fig. 7. Spatial variation of the local electrode potential during the constant current charge at 100 A from 1.6 to 2.2 V.

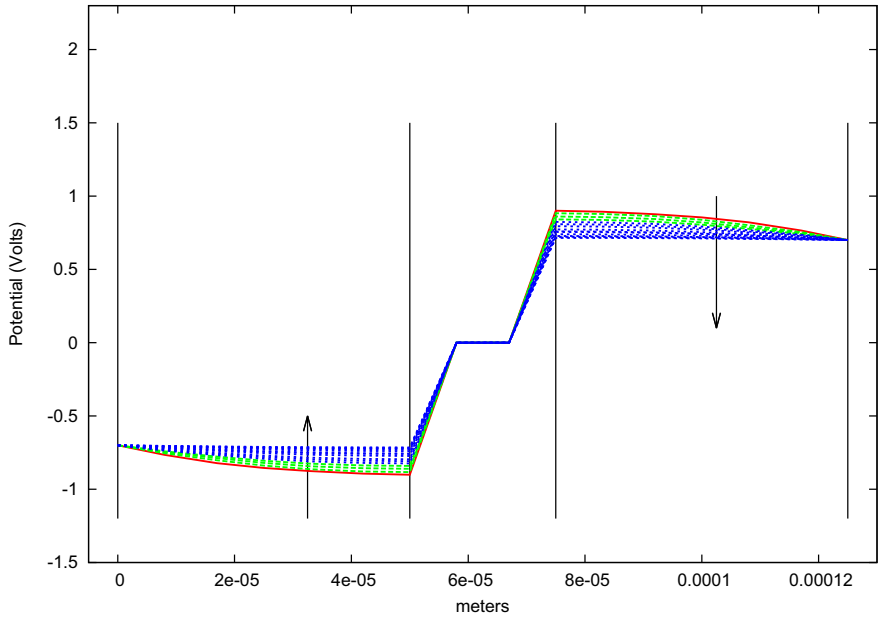

Fig. 8. Spatial variation of the local electrode potential during constant voltage discharge at 1.4 V.

mesoporous carbon the electronic conductivity ranges can be found in Ref. [40]. In Table 3, we list test cases with varying electronic conductivity and study its effect on the supercapacitor performance. As can be seen from these simulations (Fig. 9), any conductivity greater than 1.0 S m^{-1} gives almost identical results and the simulations indicate that the conductivity has to decrease to 0.1 S m^{-1} before one can see adverse affects and solid phase conductivity becomes rate limiting. From a practical perspective most carbons have electronic conductivity greater than 1.0 S m^{-1} and any further improvements in electronic conductivity would not have any improvement in overall supercapacitor performance for typical applications.

Table 3
List of cases for parametric study of σ.

Parameter	Base case	Test case-1	Test case-2	Test case-3
σ (S m^{-1})	52.1	1.0	100.0	0.1
κ (S m^{-1})	0.067	0.067	0.067	0.067
aC (F m^{-3})	86×10^6	86×10^6	86×10^6	86×10^6
ϵ_s	0.67	0.67	0.67	0.67
ϵ_l	0.6	0.6	0.6	0.6

We varied the ionic conductivity of the electrolyte as part of the next study. Ionic conductivity is usually the rate limiting step in batteries (for e.g., solid state vs. liquid electrolyte) and we wanted to explore the dependence in supercapacitors. In Table 4, we list test cases with varying ionic conductivity and study its effect on the supercapacitor performance. As in the case of batteries, the ionic conductivity turns out to be the limiting factor for charge transport, any minimal variation in the value shows a significant change in the solution and charge/discharge rates. Fig. 10 shows that energy stored and total capacity of supercapacitor is drastically low at lower values of ionic conductivities. During galvanostatic charge, the cell reaches the cut-off potential at a fraction of time at lower ionic conductivity because of the increased transport resistance and during the discharge, the limited charge stored in the capacitor is discharged over a short duration. This parametric study indicates that any improvement in the ionic conductivity can dramatically improve the supercapacitor energy density. Improving the ionic conductivity in the electrolyte is difficult and recent efforts are to improve the ion supply by electrolyte additives [41] or using transport [42]. Any improvements to ionic transport in the electrolyte can drastically improve the energy stored in a supercapacitor.

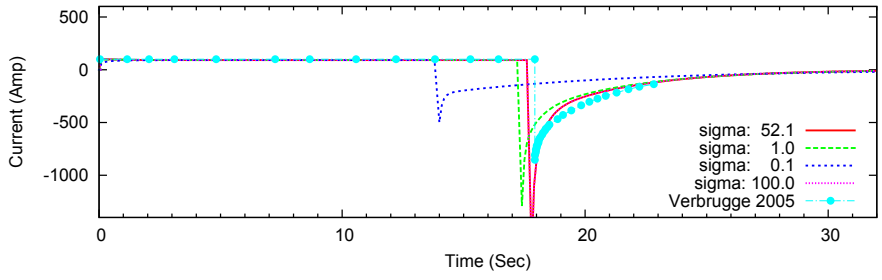

Fig. 9. Current (during galvanostatic charge and potentiostatic discharge) versus time for the parametric variation of electrode electronic conductivity σ.

Table 4
List of cases for parametric study of κ.

Parameter	Base case	Test case-1	Test case-2	Test case-3
σ (S m^{-1})	52.1	52.1	52.1	52.1
κ (S m^{-1})	0.067	0.1	0.01	0.03
aC (F m^{-3})	86×10^6	86×10^6	86×10^6	86×10^6
ϵ_s	0.67	0.67	0.67	0.67
ϵ_l	0.6	0.6	0.6	0.6

In the previous two parametric sweeps, we have changed the intrinsic transport properties of the electrode/electrolyte. The pore structure and connectivity can also influence the overall ionic and electronic conductivity. The effective transport property is proportional to ϵ^{ζ}, where ζ is the Bruggeman's coefficient. For random packed spheres, ζ is 1.5 but it is typically larger than 1.5 and can be as high as 4.0. Here we vary the Bruggeman's coefficient between 1.5–4.0 to study its effect on overall performance. The higher values of ζ implies higher tortuosity and lower effective transport coefficients. We have applied these Bruggeman's coefficient for both electronic and ionic conductivity and from the previous parametric study, the modification of ionic conductivity will have the most effect and Fig. 11 shows that the impact to performance is analogous to reduction in ionic conductivity (Fig. 10). This suggests that any reduction in tortuosity of pore structure can dramatically improve the energy stored and discharged and if these structures have nearly extremely low tortuosity ($\zeta \approx 1$) as in 1D transport, the performance can be further improved.

In the first three parametric studies, we looked at the variation of the relevant parameters controlling the transport in the electrode and electrolyte. The total capacity of the supercapacitors is directly related to specific capacitance, aC and that is the final parametric study we have conducted. Specific capacitance not only depends on the interfacial surface area to the volume but also the ability to store charge at the double layer. This parameter is highly dependent on the porosity of the electrode, the pore structure, the size of the pores, the chemical composition of the electrode and electrolyte and defines the total capacity or energy that can be stored in the supercapacitor. In this study, we picked three values for aC as shown in Table 5. As expected (Fig. 12), increasing the capacity increases the energy stored in the supercapacitor and decreasing the capacity as the opposite effect. This is a linear relationship if everything else is a constant and there are several ongoing efforts to increase the specific capacity (e.g., [14,41]).

3.3. 2D and 3D effects

3.3.1. Anisotropy

Physical characteristics such as anisotropy in various transport properties (e.g., electronic conductivity) can have significant effects in terms of local variation of the electrode/electrolyte potentials, current densities, species concentration, etc. From a system perspective, it is important to understand how that impacts the overall cell performance and efficiency. For e.g., various mesoporous carbon materials show unusually high anisotropic electronic conduction from in-plane conduction versus the through-thickness conduction. We employ the formulation we have developed to these scenarios as we can explicitly account for anisotropy and look at system level performance. In Fig. 13, we compare the overall cell performance as a function of time for the isotropic and anisotropic case. In the anisotropic case, we have assumed an extreme case where $\sigma_{xx} = 52.1$ S m^{-1} and $\sigma_{yy} = \sigma_{zz} = \sigma_{xx}/100$. Even in this extreme case, the anisotropic electronic conductivity does not have much impact on the cell performance as the transport is predominantly in the 1D x direction and lateral components do not affect the overall cell performance. In addition, as shown in previous section, electronic conductivity is not the rate limiting property

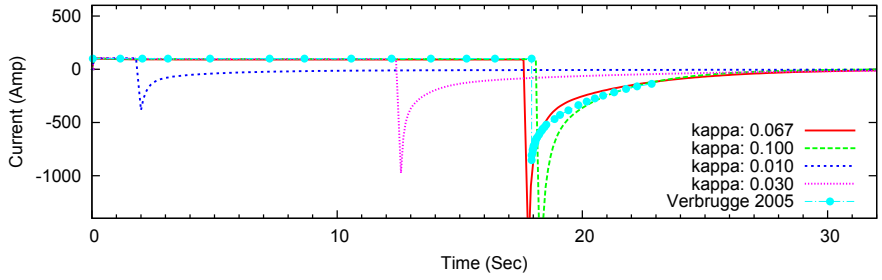

Fig. 10. Current (during galvanostatic charge and potentiostatic discharge) versus time for the parametric variation of electrolyte ionic conductivity κ.

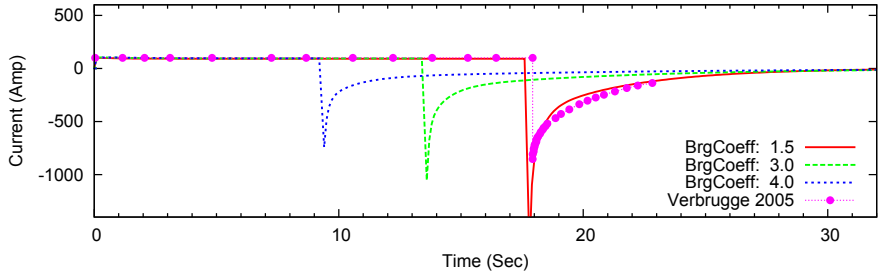

Fig. 11. Current (during galvanostatic charge and potentiostatic discharge) versus time for the parametric variation of Bruggeman's coefficient.

Table 5
List of cases for parametric study of *aC*.

Parameter	Base case	Test case-1	Test case-2	Test case-3
σ (S m^{-1})	52.1	52.1	52.1	52.1
κ (S m^{-1})	0.067	0.067	0.067	0.067
aC (F m^{-3})	86×10^6	10×10^6	50×10^6	100×10^6
ϵ_s	0.67	0.67	0.67	0.67
ϵ_l	0.6	0.6	0.6	0.6

and small perturbations in electronic conductivity would not have much impact on the overall cell performance.

3.3.2. *Spatial variability of conductivity/void fraction in a 2D supercapacitor*

In this study we introduce random variation around 20% of the void fraction in the solid phase and the corresponding changes in the liquid phase. We also introduce the anisotropy to understand the interaction between spatial variability and anisotropy and the resulting gradients in the transverse direction. The Fig. 14 show contours of variation of the volume fractions (with respect to the mean volume fraction) of the solid phase.

Fig. 15 shows quantitatively the change in the solution profile at the moment of switching from charging to discharging process. The error bars indicate the % change in the standard deviation of solution compared to isotropic case with uniform void fraction. Here we note that change is prominent during the discharging process compared to the charging process. This could be because of the high gradients in the current density introduced when capacitor is switched from galvanostatic charging to potentiostatic discharging as can be seen in Fig. 16. We compare this discharging process to the isotropic case and as can be noted, the 2D Random and 2D Random with anisotropy almost have similar charge discharge profiles indicating that even 20% variability in the porosity does not have significant effect on the overall cell performance (Fig. 17).

3.3.3. *Non-planar supercapacitor*

So far we have only shown the behavior of the new formulation for planar supercapacitor configurations where a 1D formulation is sufficient to model the dominant system level processes. In this section we demonstrate the inherent ability of the current configuration to model non-planar configurations. For this purpose, we consider an alternate configuration for the supercapacitor where the current collectors are placed on the top and bottom of the negative and positive electrodes respectively (shown in Fig. 18). In this configuration the ion transport is no longer one dimensional and the multidimensional formulation has to be employed to simulate these non-planar configurations.

In Figs. 19 and 20 we compare the spatial distribution of current immediately after we switch to potentiostatic discharge between the planar configuration and non-planar configuration. In the planar configuration, the current density contour surfaces are not perfectly planar close to the current collector but quickly become planar near the separator. This indicates that the predominant ion and electron transport becomes essentially 1D even at these high discharge rates after the switch. In comparison the non-planar case has 2d curved surfaces over the entire electrode region with some straightening over the narrow separator. As one can see higher current densities closer to separator as compared to far off regions. Visually one can also see better utilization of the electrode in the 2D configuration (similar to multidimensional architectures in batteries). As in batteries, novel 2D and 3D configurations offer ways to reduce the transport distance between the positive and negative electrodes while ensuring better volumetric utilization of the electrodes. In future, we will perform optimization studies to arrive at novel configurations

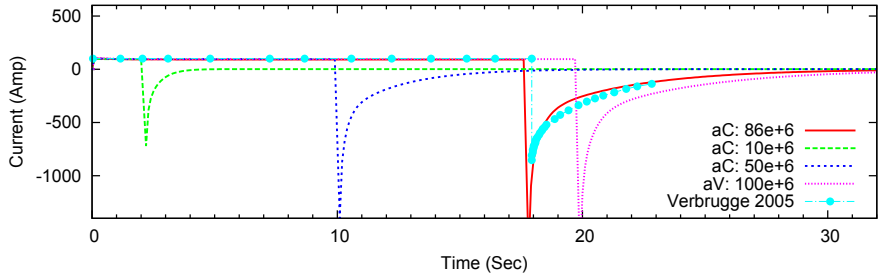

Fig. 12. Current (during galvanostatic charge and potentiostatic discharge) versus time for the parametric variation of specific capacitance (*aC*).

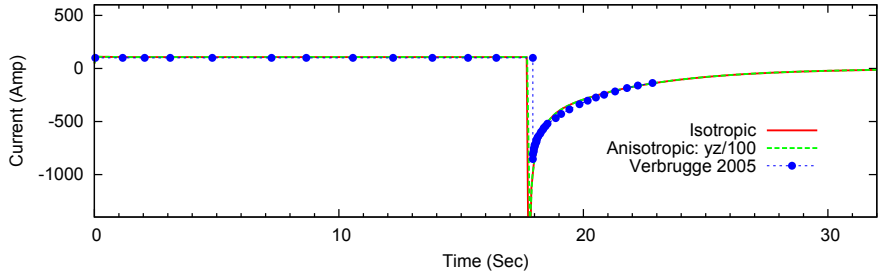

Fig. 13. Current (during galvanostatic charge and potentiostatic discharge) versus time for the anisotropic vs. isotropic electronic conductivity of the electrode.

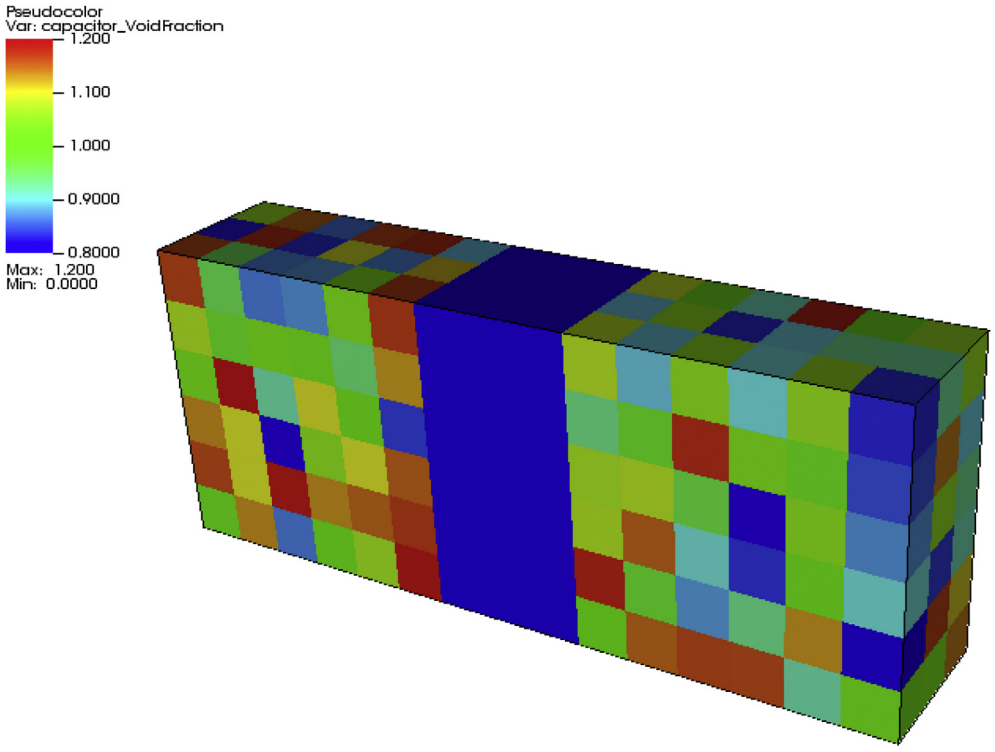

Fig. 14. Random Variations in solid phase void fractions normalize with respect to the mean volume fraction.

and it is always a challenge how one can fabricate these complex supercapacitor assemblies.

4. Conclusions

A generalized three-dimensional formulation for the electric double layer supercapacitor has been proposed, implemented, and tested in this paper. Simulation results are in very good agreement with the published experimental data. The three-dimensional nature of the charge transport and current densities at small scales due to spatial variations in porous electrodes has been revealed. These spatial variations do not have significant variations in the global response of the cell as the predominant diffusion processes smear the local effects. For standard supercapacitor with

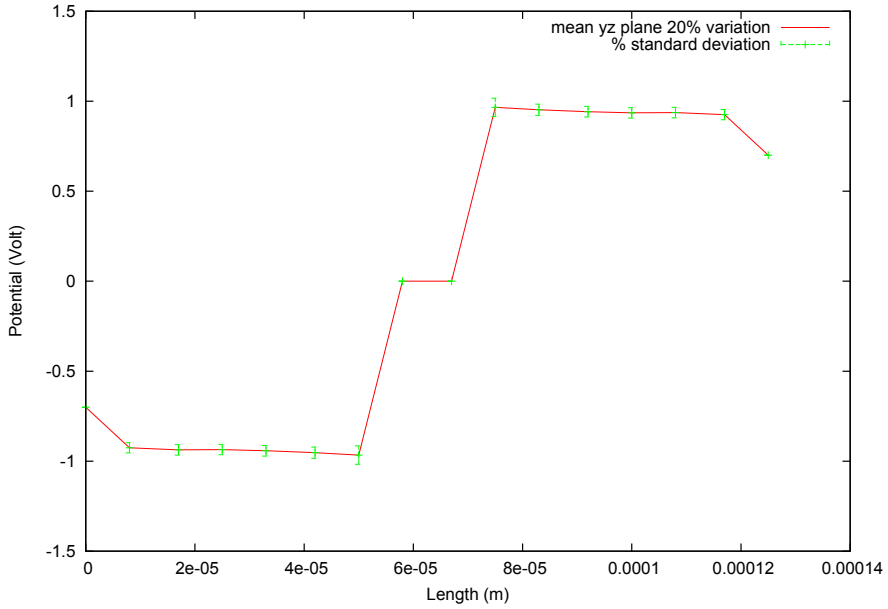

Fig. 15. Variation in the potential solution in the initial phase of the discharging process along with % deviation showing in-plane variation of the potential due to spatial variability and anisotropy.

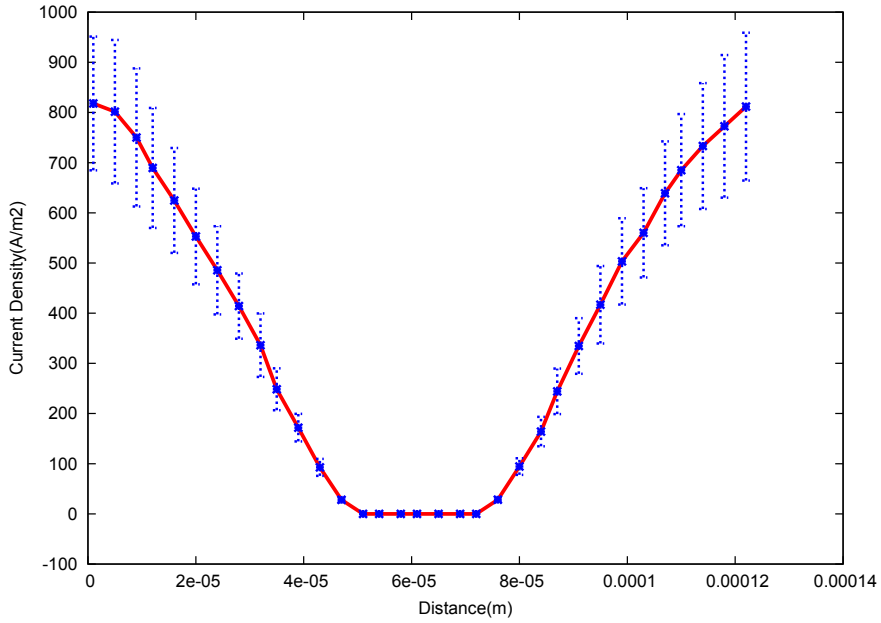

Fig. 16. Variation in current density at various X locations during the initial phase of the discharging process along with % deviation showing in-plane variation of the current density due to spatial variability and anisotropy.

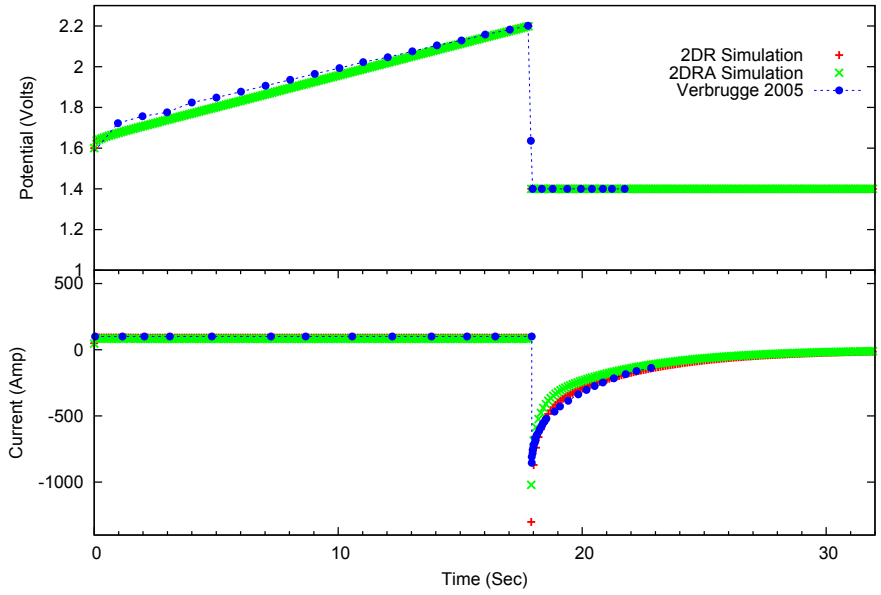

Fig. 17. Comparison of random variation of solid and liquid state void fractions.

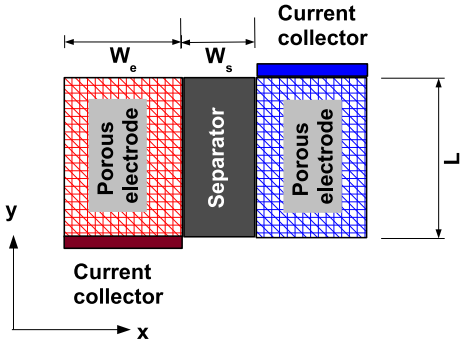

Fig. 18. Schematic of the non-planar supercapacitor.

planar electrodes, the results of the 3D model are analogous to 1D models but the generality of the 3D modeling framework can capture the local spatiotemporal variations and serve as a direct link to the material properties at the mesoscale. In addition, these models also provide the capability to design new cell configurations that provide additional flexibility to minimize the transport distance between the electrodes, packing more electrode material and thereby improving the power/energy density of the supercapacitors. In addition, the degradation is likely to be a local phenomena and having a 3D local model makes it amenable to incorporate mechanistic degradation mechanisms. It is also found from the sensitivity analysis that the supercapacitor performance is most sensitive to specific capacitance, liquid-phase ionic

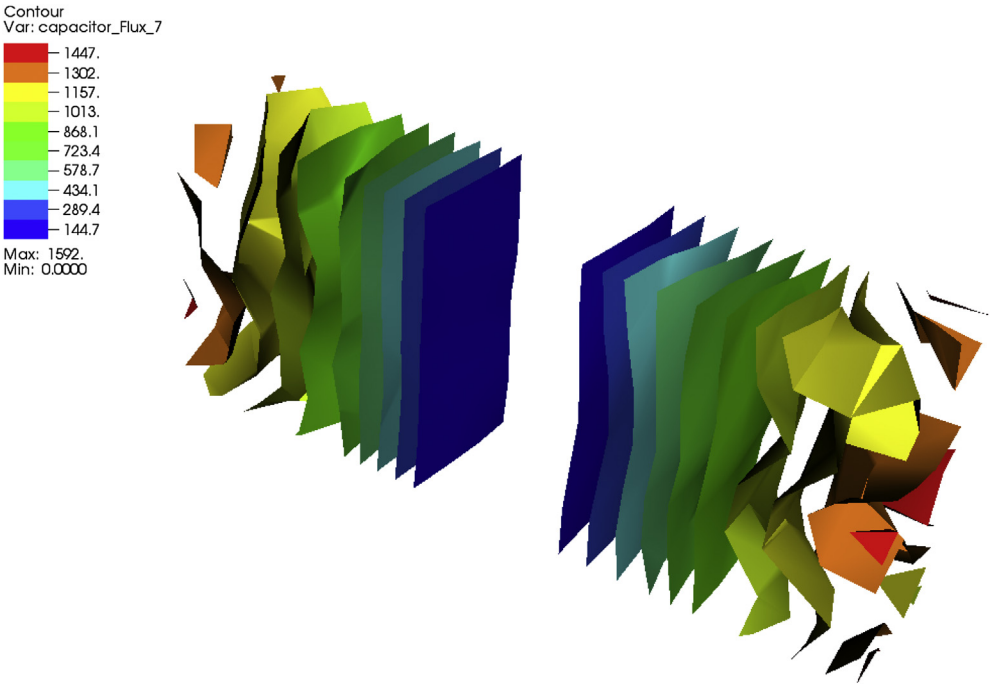

Fig. 19. Spatial distribution of the current density for parallel plate supercapacitor configuration.

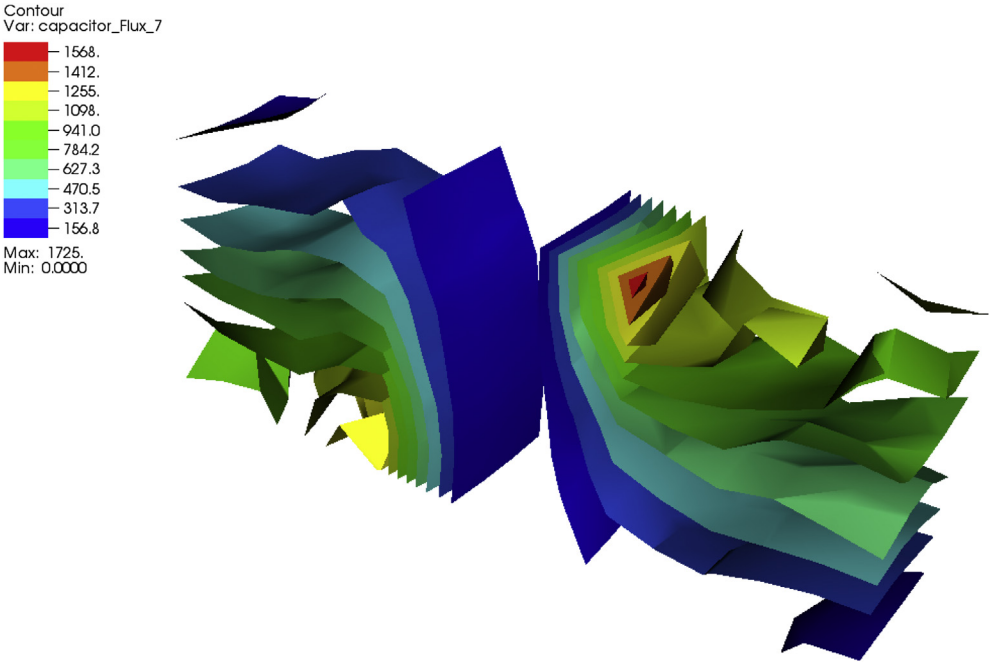

Fig. 20. Spatial distribution of the current density for non-planar supercapacitor configuration.

conductivity, and Bruggeman's coefficient. This indicates that system level improvements can be made by designing materials to have high specific capacitance, improved ionic conductivity and very low tortuous electrodes.

Acknowledgments

We would like to acknowledge the support and help from the AMP developers team in providing the back-plane and infrastructure for the multi-physics code framework. This research is supported by the Laboratory Directed Research and Development Program of Oak Ridge National Laboratory, managed by UT-Battelle, LLC, for the U. S. Department of Energy (SA, WAS, and SP). Additional support for SP was provided by Applied Mathematics Program of U. S. DOE's Advanced Scientific Computing Research (ASCR) office. BVA was funded through the ORNL/ORISE Post-doctoral Program and BP was funded by Nuclear Energy office of U. S. Department of Energy.

References

[1] A. Prosperetti, S. Sundaresan, S. Pannala, D. Zhang, Segregated Methods for Two-fluid Models, Tech. Rep., Oak Ridge National Laboratory (ORNL), 2007
[2] M. Syamlal, S. Pannala, Multiphase Continuum Formulation for Gas–Solids Reacting Flows, IGI Global, Hershey, PA, 2010.
[3] J. Newman, K. Thomas-Alyea, Electrochemical Systems, John Wiley & Sons, 2004.
[4] C.Y. Wang, W.B. Gu, B.Y. Liaw, J. Electrochem. Soc. 145 (10) (1998) 3407–3417 times cited: 61.
[5] W.B. Gu, C.Y. Wang, B.Y. Liaw, J. Electrochem. Soc. 145 (10) (1998) 3418–3427.
[6] M. Verbrugge, P. Liu, J. Electrochem. Soc. 152 (2005) D79.
[7] P. Simon, Y. Gogotsi, Nat. Mater.. ISSN: 1476-1122 7 (11) (2008) 845–854.
[8] J. Chmiola, C. Largeot, P.-L. Taberna, P. Simon, Y. Gogotsi, Science 328 (5977) (2010) 480–483.
[9] D. Pech, M. Brunet, H. Durou, P. Huang, V. Mochalin, Y. Gogotsi, P.-L. Taberna, P. Simon, Nat. Nano 5 (9) (2010) 651–654, http://dx.doi.org/10.1038/nnano.2010.162.
[10] C. Largeot, C. Portet, J. Chmiola, P.-L. Taberna, Y. Gogotsi, P. Simon, J. Am. Chem. Soc. 130 (9) (2008) 2730–2731.
[11] J. Huang, B. Sumpter, V. Meunier, Angew. Chem. Int. Ed. 47 (3) (2008a) 520–524.
[12] J. Huang, B. Sumpter, V. Meunier, Chem. - Eur. J. 14 (22) (2008b) 6614–6626.
[13] R. Signorelli, D.C. Ku, J.G. Kassakian, J.E. Schindall, Proc. IEEE 97 (11) (2009) 1837–1847.
[14] M. Hoefer, P.R. Bandaru, Appl. Phys. Lett. 95 (18) (2009) 183108–183113.
[15] J.R. Miller, R.A. Outlaw, B.C. Holloway, Electrochim. Acta 56 (28) (2011) 10443–10449.
[16] Y. Gogotsi, P. Simon, Science 334 (6058) (2011) 917–918.
[17] A. Pandolfo, A. Hollenkamp, J. Power Sources. ISSN: 0378-7753 157 (1) (2006) 11–27.
[18] G. Sikha, R. White, B. Popov, J. Electrochem. Soc. 152 (2005) A1682.
[19] C. Merlet, B. Rotenberg, P.A. Madden, P.-L. Taberna, P. Simon, Y. Gogotsi, M. Salanne, Nat. Mater. 11 (4) (2012) 306–310, http://dx.doi.org/10.1038/nmat3260.
[20] B. Conway, Electrochemical Supercapacitors: Scientific Fundamentals and Technological Applications, Springer, US, 1999.
[21] D. Futaba, K. Hata, T. Yamada, T. Hiraoka, Y. Hayamizu, Y. Kakudate, O. Tanaike, H. Hatori, M. Yumura, S. Iijima, Nat. Mater.. ISSN: 1476-1122 5 (12) (2006) 987–994.
[22] M. Stoller, S. Park, Y. Zhu, J. An, R. Ruoff, Nano Lett.. ISSN: 1530-6984 8 (10) (2008) 3498–3502.
[23] O. Lanzi, U. Landau, J. Electrochem. Soc. 137 (1990) 585.
[24] J. Gamby, P. Taberna, P. Simon, J. Fauvarque, M. Chesneau, J. Power Sources. ISSN: 0378-7753 101 (1) (2001) 109–116.
[25] A. Fuertes, F. Pico, J. Rojo, J. Power Sources. ISSN: 0378-7753 133 (2) (2004) 329–336.
[26] L. Geddes, Ann. Biomed. Eng.. ISSN: 0090-6964 25 (1) (1997) 1–14.
[27] D. Fritts, J. Electrochem. Soc. 144 (1997) 2233.
[28] R. Dougal, S. Liu, R. White, Compon. Packag. Technol. IEEE Trans.. ISSN: 1521-3331 25 (1) (2002) 120–131.
[29] V. Srinivasan, J. Weidner, J. Electrochem. Soc.. ISSN: 0013-4651 146 (1999) 1650–1658.
[30] B. Pillay, J. Newman, J. Electrochem. Soc. 143 (1996) 1806.
[31] I. Ong, J. Newman, J. Electrochem. Soc. 146 (1999) 4360.
[32] D. Dunn, J. Newman, J. Electrochem. Soc. 147 (2000) 820.
[33] C. Lin, B. Popov, H. Ploehn, J. Electrochem. Soc. 149 (2002) A167.
[34] P.P. Mukherjee, S. Pannala, J.A. Turner, Modeling and Simulation of Battery Systems, second ed., Wiley-VCH Verlag GmbH & Co. KGaA, Weinheim, 2011, pp. 843–876.
[35] K.T. Clarno, B. Philip, W.K. Cochran, R.S. Sampath, S. Allu, P. Barai, S. Simunovic, M.A. Berrill, L.J. Ott, S. Pannala, G.A. Dilts, B. Mihaila, G. Yesilyurt, J.H. Lee, J.E. Banfield, Nucl. Eng. Des.. ISSN: 0029-5493 252 (0) (2012) 108–120, http://dx.doi.org/10.1016/j.nucengdes.2012.07.018. URL, http://www.sciencedirect.com/science/article/pii/S0029549312004141.
[36] M. Sala, K. Stanley, M. Heroux, in: Proceedings of PARA'06 Conference, Umea, Sweden, 2006.
[37] H. Teng, Y. Chang, C. Hsieh, Carbon. ISSN: 0008-6223 39 (13) (2001) 1981–1987.
[38] T. Morishita, Y. Soneda, T. Tsumura, M. Inagaki, Carbon. ISSN: 0008-6223 44 (12) (2006) 2360–2367.
[39] N. Wu, S. Wang, J. Power Sources. ISSN: 0378-7753 110 (1) (2002) 233–236.
[40] S. Yoon, J. Lee, T. Hyeon, S.M. Oh, J. Electrochem. Soc. 147 (7) (2000) 2507–2512.
[41] L.-H. Su, X.-G. Zhang, C.-H. Mi, B. Gao, Y. Liu, Phys. Chem. Chem. Phys. 11 (2009) 2195–2202, http://dx.doi.org/10.1039/B814844A. URL, http://dx.doi.org/10.1039/B814844A.
[42] V. Presser, C.R. Dennison, J. Campos, K.W. Knehr, E.C. Kumbur, Y. Gogotsi, Adv. Energy Mater.. ISSN: 1614-6840 2 (7) (2012) 895–902, http://dx.doi.org/10.1002/aenm.201100768. URL, http://dx.doi.org/10.1002/aenm.201100768.